This is a preprint version of the article published by Elsevier in International Journal of Rock Mechanics and Mining Sciences, 2016.
doi:http://dx.doi.org/10.1016/j.ijrmms.2015.12.008

Characterization of Rock Slopes through Slope Mass Rating using 3D point clouds

Adrián J. Riquelme[a,1], Roberto Tomás[a], Antonio Abellán[b]

[a]*Departamento de Ingeniera Civil, Universidad de Alicante, Alicante, Spain*
[b]*Risk Analysis Group, Institut des sciences de la Terre (ISTE), Facult des Gosciences et de l'Environnement, Universit de Lausanne, Unil-Mouline, Geopolis, 1015 Lausanne, Switzerland*

Abstract

Rock mass classification systems are widely used tools for assessing the stability of rock slopes. Their calculation requires the prior quantification of several parameters during conventional fieldwork campaigns, such as the orientation of the discontinuity sets, the main properties of the existing discontinuities and the geomechanical characterisation of the intact rock mass, which can be time-consuming and an often risky task. Conversely, the use of relatively new remote sensing data for modelling the rock mass surface by means of 3D point clouds is changing the current investigation strategies in different rock slope engineering applications. In this paper, the main practical issues affecting the application of Slope Mass Rating (SMR) for the characterization of rock slopes from 3D point clouds are reviewed, using three case studies from an end-user point of view. To this end, the SMR adjustment factors, which was calculated from different sources of information and processed, using the different softwares, are compared with those calculated using conventional fieldwork data. In the presented analysis, special attention is paid to the differences between the SMR indexes derived from the 3D point cloud and

Email addresses: ariquelme@ua.es (Adrián J. Riquelme), roberto.tomas@ua.es (Roberto Tomás), antonio.abellanfernandez@unil.ch (Antonio Abellán)

URL: http://personal.ua.es/en/ariquelme (Adrián J. Riquelme), http://personal.ua.es/en/roberto-tomas (Roberto Tomás), http://www.3d-landslide.com (Antonio Abellán)

conventional field work approaches, the main factors that determine the quality of the data and some recognized practical issues. Finally, the reliability of Slope Mass Rating for the characterization of rocky slopes is highlighted.
Keywords: Geo-mechanical classifications Slope Mass Rating 3D point clouds 3D laser scanner photogrammetry failure mechanism

1. Introduction

Rock mass classification systems are well known tools which are useful for characterizing rock mass properties, in order to assign an 'index of quality' for stability purposes. These tools are used worldwide by geo-mechanical engineers in the design or pre-design stages of civil or mining projects. Existing classification systems analyse the most significant parameters responsible for influencing the behaviour of a given rock mass and providing a quantitative rating from qualitative observations. The main advantage of these classification systems is the use of straightforward (even simplistic), arithmetic algorithms for quantifying the rock mass quality. Since they have been widely applied in the past through a plethora of case studies, the use of rock mass classification systems constitute an effective way of representing the quality of the rock mass [1].

Rock Mass Rating (RMR) [2, 3] along with Q [4] is one of the most widely used rock mass classification systems [5]. This classification was initially developed for tunnels. Although the RMR index has been applied to rock slopes and foundations, its application is hard, as there is no exhaustive definition for the selection of the correction factors [6]. Based on this, Slope Mass Rating (SMR)

provides comprehensive adjustment factors to RMR system [7, 8]. These adjustment factors depend on the geometrical relationship between the rock mass discontinuities and the slope, as well as the excavation method.

The parameters required for rock mass characterization are usually acquired through time-consuming field investigation techniques: geological compass for obtaining discontinuity orientations, tape measurements for discontinuity spacings or persistence and roughness analysis by local examinations. Sometimes, fieldwork campaigns can be affected by several restrictions, being well known examples, such as, safety issues in active rockfall areas, possible access limitations and intensive work requirements in highly fractured rock masses. More recently, several attempts have been made to determine the rock mass quality using remote sensing data [9, 10] or digital pictures [11]. The use of remote techniques (for example, 3D laser scanner and digital photogrammetry) allows for the acquisition of three dimensional information of the terrain with high accuracy and high spatial resolution. Three-dimensional datasets coming from both techniques are widely used for landslide investigations [12, 13]. Moreover, the scientific community is showing an exponentially growing interest in the study of the extraction of several parameters influencing rock slope stability, including rock mass discontinuity orientations [14, 15, 16, 17, 18, 19, 20, 21, 22, 23] and other rock mass parameters: spacing between discontinuities [24, 14, 25], discontinuity persistence [26, 18, 27] and roughness [28, 26, 29, 11].

In this work, the practical issues for the characterization of rock slopes by means of the SMR index are reviewed, using three case studies. The sources of

information being used are 3DPC datasets combined with information acquired through traditional methods. Basic RMR index is calculated, using the fieldwork data. The main aim of this work, is the analysis of SMR adjustment factors, and how the use of the different sources of information affect SMR index, and thus, the slope of characterization. To achieve this, an open source tool, has been developed. It is programmed in MATLAB, and is able to calculate the SMR adjustment factors, including the auxiliary angles and their graphical interpretation.

This paper, has been organised in the following way: (a) An explanation of the methodology used, which is included in §2; (b) A description of the three case studies in which the method is applied at §3; (c) An application of the three case studies is presented at §4; and finally, (d) A summary of the results along with a discussion of the developed approach is presented at §5 and §6, respectively.

2. Proposed methodology approach

2.1. General overview

The methodology presented in Figure 1 uses 3D Point Clouds (which would be subsequently called 3DPC in this work), which is acquired, by remote imaging techniques (that is 3D laser scanner or digital photogrammetry) and the basic RMR parameters, obtained by means of conventional field surveys as input data. The calculation of SMR is performed following three main steps: (a) 3D data acquisition, (b) Extraction of geometrical information, and (c) Computation of SMR value, as explained below:

The first step consists of the 3D data acquisition. First, the studied rock slope

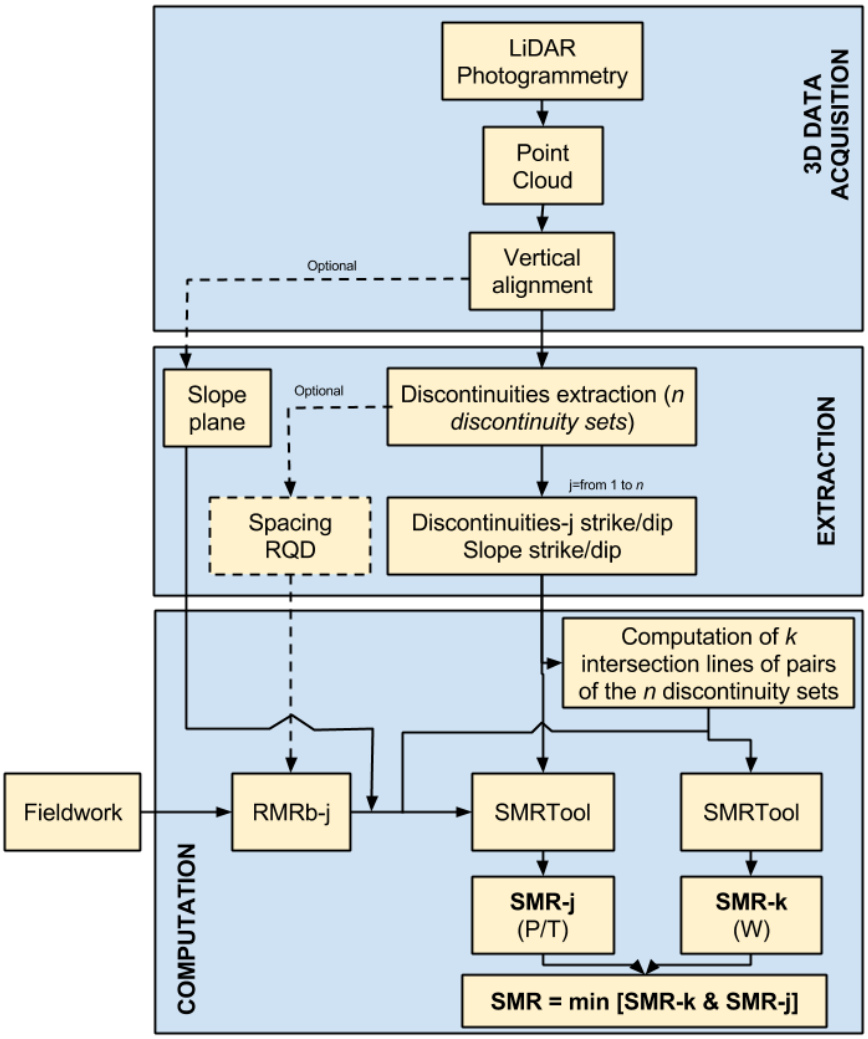

Figure 1: Flowchart of the methodology used. P: planar failure; T: Toppling failure; W: wedge failure.

is geometrically modelled by means of a 3DPC which can be acquired by means of 3D laser scanner or digital photogrammetry techniques [30, 31]. Then, the PC is vertically aligned with the global reference system, in order to correctly extract the dip of the discontinuity planes. The PC can also be properly oriented to the north, although, this last step is not mandatory when working on a relatively sloped-discontinuity reference system.

The extraction of parameters is performed in the second step. The PC is analysed by an accepted and reliable method, and is used, to extract the discontinuity sets. After that, each point from the PC is classified into its corresponding mean orientation or Discontinuity Set (subsequently called DS) and plane. In this step, the slope orientation (dip and dip direction) is also derived from the 3DPC fitting, which is a representative plane of the slope. Although, the orientation of the slope can also be measured during fieldwork by using a geological compass, it is recommended to derive the slope of the plane from the 3DPC, in order to have both the slope and the discontinuities referred to in the same reference system.

The SMR index is computed in the last step. A kinematic analysis is performed for each DS and/or for each pair of discontinuity extracted in step two. This information allows for the computation of SMR for each discontinuity set or combination of discontinuities by means of the SMRTool [32], which provides a graphical interpretation of the potential failure mechanisms, the outputs of the SMR value and the recommendations proposed by Romana [7].

2.2. Extracting discontinuity and slope orientation

Despite different approaches and software products can be used at this stage (for exemple, PlaneDetect, SplitFX, PCM, DiAna or Coltop3D), the open source software Discontinuity Set Extractor (DSE, available on http://personal.ua.es/en/ariquelme/) [23] was used to complete this work. This software semi-automatically extracts DS, assigns a DS to each point and extracts different planes for each DS (subsequently referred to as cluster). Finally, in this work, the orientation and the position of each cluster are calculated. In this work, the application of 3DPC to SMR calculation is analysed, and DSE results are compared using the those obtained with PlaneDetect software.

The slope plane (that is, the mean excavation surface) can also be extracted from the 3DPC fitting plane. Alternatively, it can be measured in the field or defined during design state, when the slope has not been excavated.

2.3. Slope Mass Rating (SMR) computation

SMR index is calculated by applying four adjustment factors to the RMR_b : F_1, F_2, F_3 and F_4. These factors depend both on the slope excavation method and on the geometrical relationships that exist between the slope and the discontinuities affecting the rock mass [7]. The SMR index is computed, using the following formula:

$$SMR = RMR_b + (F_1 \times F_2 \times F_3) + F_4 \tag{1}$$

Where:

RMR_b is the RMR basic parameter in the RMR geomechanical classification [3]. The maximum value that RMR_b can reach is 100, which means a high quality rock mass from a rock mechanics perspective. As a reminder, basic RMR is computed using the following formula:

$$RMR_b = X_1 + X_2 + X_3 + X_4 + X_5 \tag{2}$$

where X_1 to X_5 is assigned a value, which depends on the characteristics of the rock or the discontinuities. The maximum values that these factors (X_i) can reach, jointly with their relative weights and the possible data sources for obtaining these parameters, are shown in Table 1.

F_1 parameter depends on the angular relationship between the dip direction of the considered discontinuity and the slope (see parameter A in Table 2).

F_2 parameter, depends on the failure mechanism, as follows: (a) For a planar failure mechanism along a single discontinuity, F_2 depends on the dip of the discontinuity (see parameter B in Table 2); (b) For a wedge failure mechanism between two given discontinuities, F_2 depends on the plunge of the line of intersection of the discontinuities; (c) Finally, for toppling failure mechanism the parameter F_2 adopts a unitary value. For planar and wedge mechanisms, F_2 is related to the discontinuity shear strength [8].

F_3 parameter also depends on the failure mechanism, as follows: (a) for planar and toppling failure mechanism, F_3 depends on the angular relationship existing between the slope dip and the dip of the discontinuity (see parameter C in Table 2);

Table 1: Basic RMR parameters and their plausible data sources.

Parameter (eq. (2))	Weight	Acquisition	Data source
X_1: Strength of intact rock material	15	PLT, Uniaxial compressive strength	Field, laboratory
X_2: Drill core Quality RQD	20	Drill core, geometric analysis	Field, 3D
X_3: Spacing of discontinuities	20	Drill core, geometric analysis	Field, 3D
X_4: Condition of discontinuities:	30		
- Discontinuity Length	6	Geometric analysis	Field, 3D
- Separation (aperture)	6	Geometric analysis	Field, 3D
- Roughness	6	Geometric analysis	Field, 3D
- Infilling (gouge)	6	Geometric analysis	Field, images
- Weathering	6	Visual inspection	Field, images
X_5: Ground water	15	Visual inspection	Field

(b) for wedge failure mechanism, this parameter can be calculated as the existing angle between the slope dip and the plunge of the intersection line between the two considered discontinuities. This parameter, which expresses the probability of discontinuity outcropping on the slope face [8], varies from 0 to 60 points.

F_4 parameter depends on the method of excavation used for the studied slope (see Table 2).

Consequently, the adjustment factors F_1, F_2 and F_3 can be deduced from the following geometrical data: (a) Strike (or alternatively dip direction) of the slope and each DS; (b) Dip of each DS and dip of the slope, and (c) When a wedge failure mechanism can occur, trend and plunge of the intersection line between the two planes are also required [33].

The calculation of the above described geometrical parameters require a previous interpretation of the relative position of the discontinuity planes and the slope for a planar failure mechanism, as well as the line of intersection between two planes in the case of a wedge mechanism. Then, the failure mode which is ac-

Table 2: Adjustment factors for SMR. P: planar failure; T: toppling failure; W: wedge failure. F_1: parallelism between joints and slope; F_2: dip angle in the planar mode of failure; F_3: relationship between slope and joints dips α_j: dip direction of the discontinuity; α_s: dip direction of the slope; α_i: trend of the intersection line of two sets of discontinuities; β_s: slope dip; β_j: discontinuity dip; β_i: plunge of the intersection line of two sets of discontinuities. Modified from [34] and [33]

	Type of failure		Auxiliary angles	Very favorable	Favorable	Normal	Unfavorable	Very unfavorable
Parallelism	P	A=	$\lvert\alpha_j - \alpha_s\rvert$	> 30°	30 – 20°	20 – 10°	10 – 5°	< 5°
	T		$\lvert\alpha_j - \alpha_s - 180\rvert$					
	W		$\lvert\alpha_i - \alpha_s\rvert$					
	P/T/W	F_1		0.15	0.40	0.70	0.85	1.00
Dip angle	P/W	B=	β_j or β_i	< 20°	20 – 30°	30 – 35°	35 – 45°	> 45°
	P/W	F_2		0.15	0.40	0.70	0.85	1.00
	T					1.00		
Dip relationship	P	C=	$\beta_j - \beta_s$	> 10°	10 – 0°	0°	0 – (−10)°	< (−10)°
	W		$\beta_i - \beta_s$					
	T		$\beta_j + \beta_s$	< 110°	110 – 120°	> 120°	-	-
	P/T/W	F_3		0	-6	-25	-50	-60

Excavation method (F_4)			
Natural slope	+15	Blasting or mechanical	0
Presplitting	+10	Deficient blasting	-8
Smooth blasting	+8		

tually compatible with the existing relative geometry between the slope and the discontinuities is determined. Subsequently, the SMR parameters are calculated following Table 2.

For a systematic computation of the SMR adjustment factors, the different failure mechanisms are determined considering the following general geometrical conditions: for planar failure: $|\alpha_j - \alpha_s| < 90°$; for wedge failure: $|\alpha_i - \alpha_s| < 90°$; and for toppling failure: $|\alpha_j - \alpha_s| > 90°$; where α_j and α_s are the dip direction of the discontinuity and of the slope, respectively, and α_i is the dip direction of the

intersection line of the wedge. Note that this criterion has been stated according to Romana [8] and only considers the geometrical condition, necessary for the development of the different types of failure.

2.4. SMRTool description

The geometrical conditions for the computation of the SMR index (see Figure 2) have been implemented in an open source software named SMRTool [32] (available on http://personal.ua.es/en/ariquelme/). The inputs of this software are, the orientations of the slope, the discontinuities and their corresponding RMR_b values. Wedges are automatically calculated, indicating the pair of intersecting discontinuities. SMRtool software shows the angular relationship between the discontinuities and the slope as well as a graph to visualize them. Finally, adjustment factors using discrete and continuous functions and Romana's recommendations are automatically displayed. This software aids users, in interpreting the calculation of the adjustment factors and all auxiliary angles in an intuitive, analytical and graphical mode.

3. Case studies

The proposed methodology was applied to the three different case studies, which are described in this section. This analysis, aims to highlight the main advantages and shortcomings of using 3DPC in evaluating the geomechanical quality of rocky slopes through SMR.

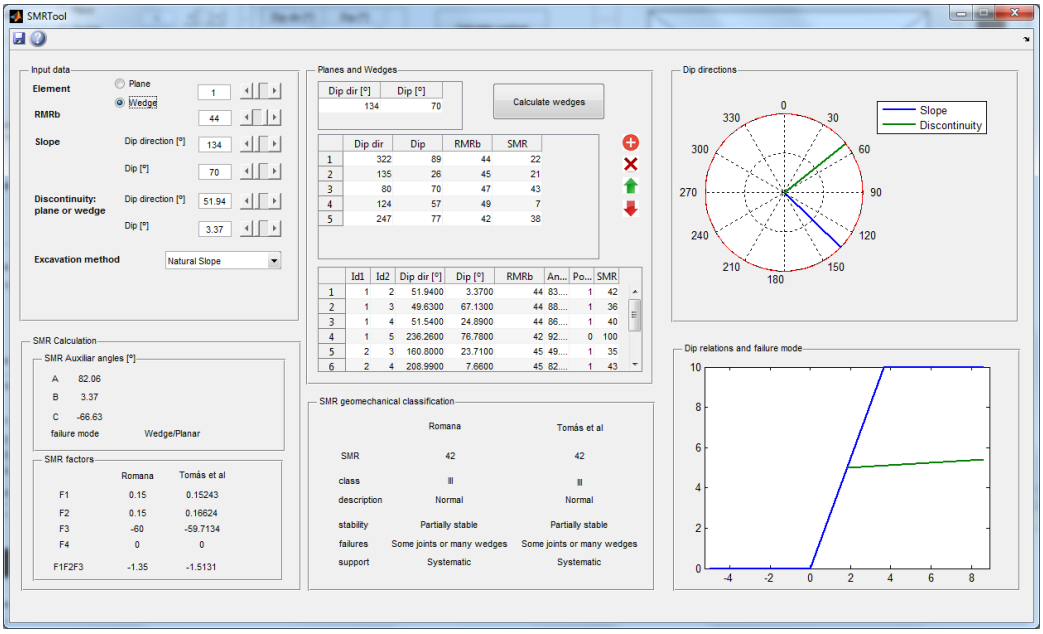

Figure 2: Screenshot of the SMRTool [32] (freely available on the author's website).

3.1. Case study I: Rockbench repository, Kingston (Canada)

The main aim of this first case study is to calculate the SMR factors of a rocky slope, by using different sources of information and different analysis approaches [22], to analyse their main practical advantages and disadvantages. The source of the data consists of a 3D point cloud from a rocky slope, on a highway road near Kingston, Canada, which is available on the online repository Rockbench [31].

This outcrop consists of granites with very well defined planes of discontinuity. This outcrop was already analysed by means of traditional compass measurements and by using the PlaneDetect software [22]. This slope can be divided into three separated sectors with different orientations. Since any RMRb value is publicly available for this case study, the comparison between different methods

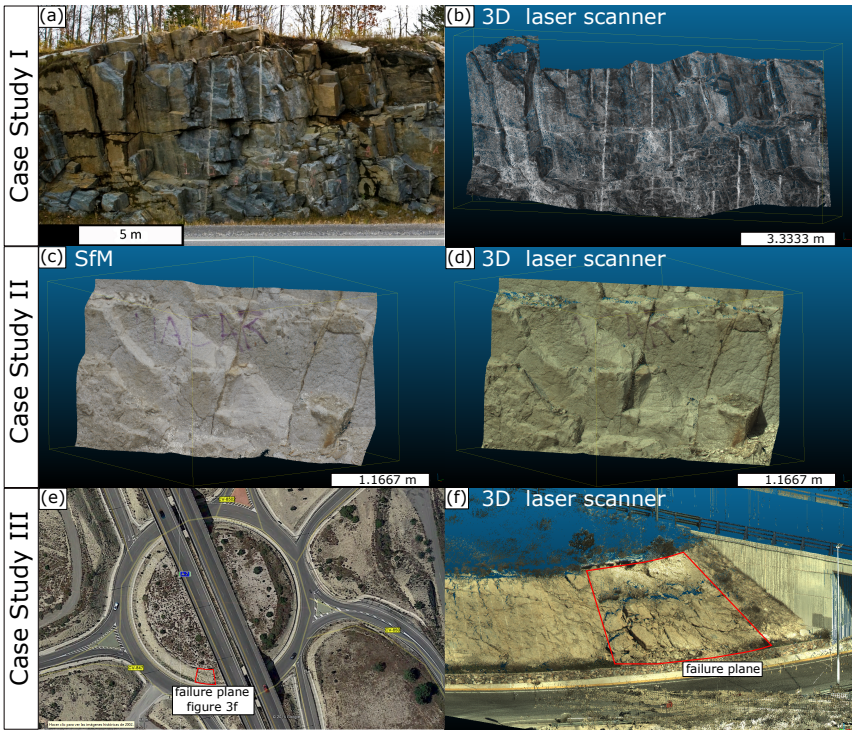

Figure 3: Case Study I: (a) Picture of the rock slope, Kingston (Canada); (b) Section of the previous picture showing the analysed 3DPC; case study II: (c) 3DPC acquired by digital photogrammetry; (d) 3D point cloud acquired by 3D laser scanner; case study III: (e) Orthographic image (Google Earth, imagery date: June 30th, 2013); (f) 3DPC view

has been performed in terms of the SMR adjustment factors. To achieve this, we utilized the discontinuities extracted in [22] and the discontinuities detected in this work (see section 4).

3.2. Case study II: Application of the methodology to compute SMR to an urban rock slope.

The second case study aims to calculate SMR by using the 3DPC on a slope that was acquired by two different surveying techniques: the 3D laser scanning and multi-image photogrammetric techniques (SfM). This information is complemented with the data acquired from the fieldwork (for example, weathering, roughness, infilling, aperture, spacing and persistence) to compute basic RMR.

The slope is located in Alicante (SE Spain) and is composed of marls, argillaceous limestones and calcareous limestones. This rock mass presents some practical difficulties for its characterization based on three main reasons: (a) Most of the discontinuity surfaces are smoothed by weathering; (b) The strata is slightly folded and has been affected by several normal faults and (c) The sub-horizontal surfaces are partially (or even completely) covered by debris due to the progressive degradation of the materials located at the upper part of the slope. Consequently, a representative outcrop of the rock mass has been selected to minimize these mentioned effects that can mask the true discontinuity surfaces. The slope was excavated by mechanical methods.

The pictures acquired for the application of the SfM were performed using a Canon EOS 550D digital camera on June 6th, 2014. Then, the 3DPC was gener-

ated using the Agisoft Photoscan software and ground control points were taken, from a previously registered 3D laser scanner dataset, acquired on August 2nd, 2012. In order to avoid some of the inconveniences mentioned in the previous paragraph (that is, a and b), a 3x2 meter sector was studied (Figure 3 c and d) and is defined by 835752 points (a point density of $14x10^4 pts/m^2$). The second model was acquired by a laser scanning survey carried out on March 28th, 2015 with a Leica C10 laser scanner. In order to reduce shadow areas, it was carried out in three separate stations and the point cloud was registered using data from a digital map (SIGNA http://signa.ign.es/signa/). The studied sector was subsampled obtaining a point cloud of 301089 points (a point density of $8x10^4 pts/m^2$).

3.3. Case study III: Application of the methodology to a roundabout slope on A-7 highway (Alicante, Spain)

The last case study focuses on the slope stability of a roundabout excavation in which the slope strike varies from 0° to 360° (see Figure 3 e and f). The roundabout is located on the road CV-8502 intersection with CV-847 in Alicante (SE Spain) under the A-7 highway. The lithology of the studied slopes consist of Paleogene marly limestones [35]. The south slope of this roundabout was affected by a planar failure after its excavation (see Figure 3 e and f).

In this case study the discontinuities are derived from the 3DPC obtained by means of a 3D laser scanner, and the roundabout slope is modelled by a synthetic 3D point cloud. Data was acquired by means of a 3D laser scanner, Leica Scanstation C10, by three different scans on November 4th, 2014 with a density

of $5223 pts/m^2$ (see Figure 3f).

Since the SMR adjustment factors vary depending on the DS orientations (that is, dip and dip direction), and the basic RMR is considered constant for each DS, thus, in this case, the SMR index only varies depending on the slope plane orientation. Therefore, a synthetic slope surface excavation, has been generated, which assigns a constant slope dip direction and a variable dip for each point of this synthetic surface to calculate the SMR. Note that the slope's PC has not been generated from the 3D laser scanner, but from the known parametric surface. This process is defined in a similar way to those of the earlier design stages in which the slope had not been excavated, but its orientation was defined by the project.

4. Results

4.1. Results of case study I

The results of the 3DPC got from this slope, was analysed by means of the DSE software [23], by extracting the discontinuity sets shown in Figure 4a and computing the wedges generated by the intersection of the pairs of planes. Thereafter, the results were compared with those derived from the 3DPC, using other methods (PlaneDetect software, 3D laser scanning datasets and digital photogrammetry datasets) and conventional field surveys (Figure 4b). The results of the comparison are summarized in Table 3 and a basic statistical analysis is shown in Figure 5. Figures 5 a, b and c show the comparison between the SMR adjustment factors contribution $F_1 x F_2 x F_3 + F_4$, which was calculated using fieldwork data (X-axis) and 3D point clouds for each slope (Y-axis). In this figure, the line that

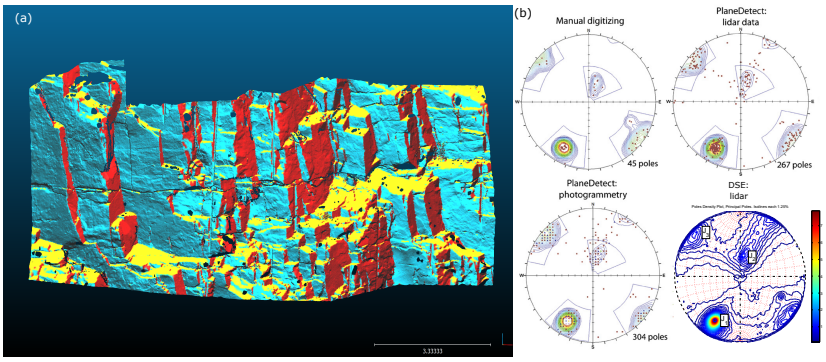

Figure 4: Case study I. (a) Classified point cloud, one colour per DS using DSE software; (b) Poles density of normal vectors for each source of information. Stereoplots using fieldwork datasets and PlaneDetect software have been obtained from [22].

bisects X-axis and Y-axis shows those points where there is no variation in the SMR values in terms of adjustment factors. This line shows those cases, where the contribution of the SMR adjustment factors, using a specific remote acquisition technique, is equal to the one obtained using fieldwork data. Additionally, two parallel lines have been depicted indicating those values for which there is a class variation in the SMR index. Therefore, this figure shows the existing differences in the $F_1xF_2xF_3 + F_4$ term, for the different sources of information against those calculated using field data. Figures 5 d, e and f summarize the adjustment factors contribution for each discontinuity set in a box-and-whisker plot depicting graphically, the groups of adjustment factor terms through their quartiles. In this figure, it is observed that previous term varies significantly for certain planes depending on the source of information and the applied approach.

Table 3: Case study I. Calculation of the SMR correction factors ($F_1xF_2xF_3+F_4$) of the studied rock slope by means of the proposed methodology from different data acquisition methods (i.e. geological compass, LiDAR and photogrammetry) and techniques of analysis (i.e. Plane detect and DSE).

		J_1	J_2	J_3	W_{12}	W_{13}	W_{23}
dip direction / dip	Manual Geological Compass	(028/76)	(307/86)	(205/30)	(021/76)	(117/01)	(219/29)
	Plane Detect LiDAR	(029/75)	(308/89)	(198/32)	(034/75)	(117/06)	(218/30)
	Plane Detect Photogrammetry	(029/76)	(309/90)	(194/34)	(039/76)	(117/08)	(219/31)
	DSE LiDAR	(030/75)	(135/87)	(187/33)	(055/73)	(116/12)	(223/28)
Slope 1: (008/88)	Manual Geological Compass	-24,00	-7,50	-4,20	-42,00	0,00	0,00
	Plane Detect LiDAR	-24,00	-0,90	-17,50	-24,00	0,00	0,00
	Plane Detect Photogrammetry	-24,00	-0,90	-21,25	-9,00	0,00	0,00
	DSE LiDAR	-24,00	-3,75	-25,00	-9,00	0,00	0,00
Slope 2: (162/77)	Manual Geological Compass	-3,75	-3,75	-3,60	0,00	-1,35	-3,60
	Plane Detect LiDAR	-3,75	-3,75	-6,30	0,00	-1,35	-6,30
	Plane Detect Photogrammetry	-3,75	-3,75	-6,30	0,00	-1,35	-6,30
	DSE LiDAR	-3,75	-2,40	-16,80	0,00	-1,35	-3,60
Slope 3: (186/88)	Manual Geological Compass	-10,00	-3,75	-16,80	0,00	-1,35	-3,60
	Plane Detect LiDAR	-10,00	-3,75	-29,40	0,00	-1,35	-6,30
	Plane Detect Photogrammetry	-10,00	-3,75	-35,70	0,00	-1,35	-6,30
	DSE LiDAR	-10,00	-7,50	-42,00	0,00	-1,35	-3,60

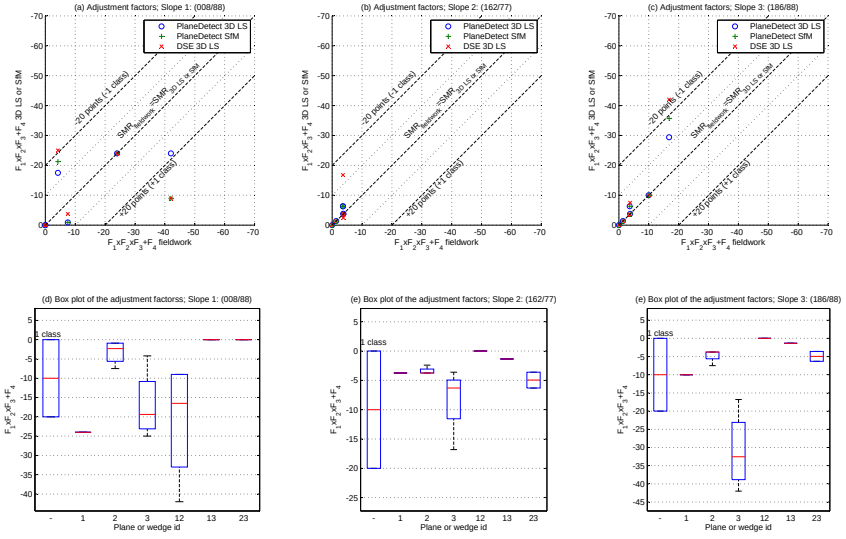

Figure 5: Case study I. (a) to (c) Comparison of adjustment factors obtained with fieldwork data versus those obtained with 3D point clouds for each slope. (d) to (f) Box whisker plot for all sources of information and each slope.

4.2. Results of case study II

In this case study the SMR index has been calculated using fieldwork measurements, as well as 3D laser scanners and SfM data sets have been analysed by means of DSE software. In both cases, five discontinuity sets were obtained, but one of them was discarded, as it was surface generated as a result of weathering processes. Figures 6 c and e show the classified point cloud and Figures 6 b, d and f show their respective normal vector's pole density and the extracted discontinuity sets. The slope plane was extracted by its best fit plane (133/72). Finally, all wedges were calculated and only those whose trend and slope's dip direction formed an angle lower than 90° were selected as potential wedges.

In this case study, RMRb values were computed, using data acquired from the field. Their values are summarized in Table 4. All SMR values were calculated using the SMRTool software. Figure 7a shows the comparison between SMR computed from fieldwork and SMR computed from 3DPC. Additionally, the results were compared with each plane or wedge in a box plot (see Figure 7).

4.3. Results of case study III

For this case study, two different methods were used: (a) In method, three discontinuity sets were detected through classical fieldwork: (J_1, J_2 and J_3) ; (b) Using the second method, an additional discontinuity set was extracted (J_4), when investigating the 3DPC using DSE software. The RMRb was calculated during fieldwork from the data collected manually, and in a complementary way, from the information extracted from the DSE (see Table 5).

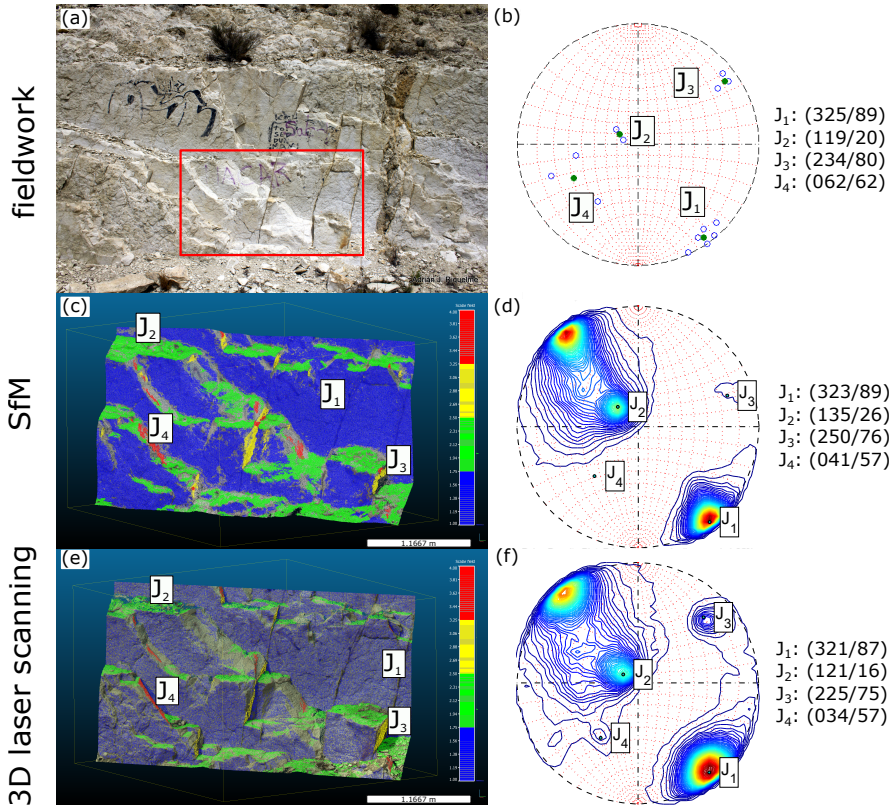

Figure 6: Case study II:. (a) Picture of the slope; (b) compass measurements and mean planes; (c) SfM classified point cloud; (d) Normal vector poles' density; (e) 3D laser scanner classified point cloud; (f) Normal vector's point density.

Table 4: Case study II. SMR Calculations of all discontinuity sets and wedges using different sources of information: SfM datasets, 3D laser scanning datasets and fieldwork.

	plane/ wedge id	dip dir [°]	dip [°]	RMR_b	A [°]	B [°]	C [°]	type of failure	F_1	F_2	F_3	F_4	SMR	Class
SfM dataset	J_1	323	89	44	10	89	161	Toppling	0.70	1.00	-25	0	26	IV
	J_2	135	26	45	2	26	-46	Planar	1.00	0.40	-60	0	21	IV
	J_3	250	76	42	63	76	148	Toppling	0.15	1.00	-25	0	38	IV
	J_4	41	57	47	88	57	129	Toppling	0.15	1.00	-25	0	43	III
	W_{12}	53	4	44	80	4	-68	Wedge	0.15	0.15	-60	0	42	III
	W_{14}	51	57	44	82	57	-15	Wedge	0.15	1.00	-60	0	35	IV
	W_{23}	166	23	42	33	23	-49	Wedge	0.15	0.40	-60	0	38	IV
	W_{24}	114	24	45	19	24	-48	Wedge	0.70	0.40	-60	0	28	IV
3D laser scanning	J_1	321	87	44	8	87	159	Toppling	0.85	1.00	-25	0	22	IV
	J_2	121	16	45	12	16	-56	Planar	0.70	0.15	-60	0	38	IV
	J_3	225	75	42	88	75	147	Toppling	0.15	1.00	-25	0	38	IV
	J_4	34	57	47	81	57	129	Toppling	0.15	1.00	-25	0	43	III
	W_{12}	51	6	44	82	6	-66	Wedge	0.15	0.15	-60	0	42	III
	W_{14}	46	56	44	87	56	-16	Wedge	0.15	1.00	-60	0	35	IV
	W_{23}	139	15	42	6	15	-57	Wedge	0.85	0.15	-60	0	34	IV
	W_{24}	113	16	45	20	16	-56	Wedge	0.70	0.15	-60	0	38	IV
fieldwork	J_1	325	87	44	12	87	159	Toppling	0.7	1.00	-25	0	26	IV
	J_2	119	20	45	14	20	-52	Planar	0.7	0.15	-60	0	38	IV
	J_3	234	83	42	79	83	155	Toppling	0.15	1.00	-25	0	38	IV
	J_4	62	62	47	71	62	-10	Planar	0.15	1.00	-60	0	38	IV
	W_{12}	55	9	44	78	9	-63	Wedge	0.15	0.15	-60	0	42	III
	W_{14}	49	61	44	84	61	-11	Wedge	0.15	1.00	-60	0	35	IV
	W_{23}	146	18	42	13	18	-54	Wedge	0.70	0.15	-60	0	35	IV
	W_{24}	142	19	45	9	19	-53	Wedge	0.85	0.15	-60	0	37	IV
	W_{34}	145	12	42	12	12	-60	Wedge	0.70	0.15	-60	0	35	IV

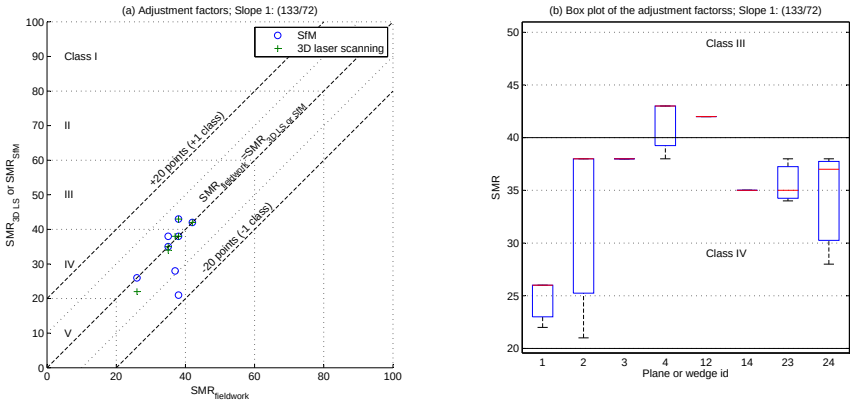

Figure 7: Case study II. (a) Comparison of adjustment factors obtained with fieldwork data versus those obtained with 3D point clouds; (b) box whisker plot for the three sources of information: fieldwork, SfM and 3D laser scanner.

In this case study, the slope orientation varied around the roundabout adopting different dip directions from 0 to 360° and having a constant dip. SMR index was calculated for all orientations of the roundabout, assuming that the slope of the roundabout defined a conical frustum, whose angle was equal to the slope dip (that is, 50°).

First of all, SMR computation for planar failure mechanisms was carried out. Figures 8 a to f show the result of SMR index calculation, where the values for each slope sector are depicted in a different colour according to the colour bar scale (0 and 70 for the lowest and highest values, respectively). Figures 8 b, c, d and e show the SMR index values of the discontinuity sets J_1, J_2, J_3 and J_4, being the Figure 8f the minimum envelope of all the SMR values calculated for the different DS. This last figure shows that the lowest SMR index value is 11, which implies a very bad (Class V) and 'completely unstable' slope according to Romana's classification system [8]. The SMR index for this specific location is calculated in details in Table 5.

Additionally, a wedge failure mechanism was also analysed following the previously described procedure. The minimum values of the SMR index were 30 in the West and South East parts of the slope (see Figure 8i). Thus, when analysing the different SMR index computations it can be observed that the minimum value of the SMR index was computed at the sector of the slope, where a planar slide had occurred (see Figure 3). Therefore, this case study highlights the usefulness and reliability of the SMR index to map areas of lower geomechanical quality, in which failures are more likely to occur.

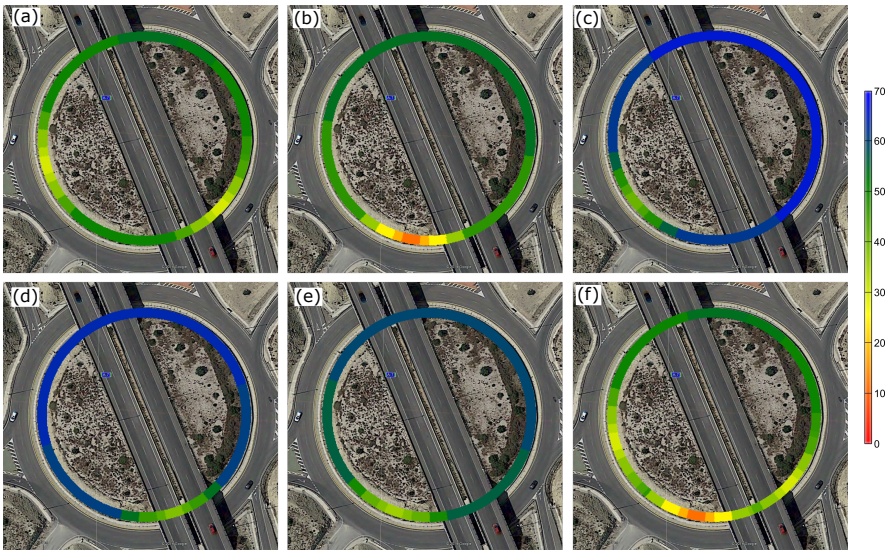

Figure 8: Case study III: Orthographic view of the slope acquired from Google Maps, imagery date: June 6th, 2013; (a) Envelope of minimum SMR associated to wedge failure mechanism; Figures (b) to (e) SMR values of each point of the conical frustum corresponding to both planar and toppling failure mechanisms; (f) envelope of the minimum SMR values.

Table 5: Case study III. SMR Calculations of all discontinuity sets and wedges at the failure plane (190/50).

plane/ wedge id	dip dir [°]	dip [°]	RMRb	A [°]	B [°]	C [°]	failure	F_1	F_2	F_3	F_4	SMR	Class
J_1	190	45	54	0	45	-5	Planar	1.00	0.85	-50	0	11	V
J_2	52	73	66	42	73	123	Toppling	0.15	1.00	-25	0	62	II
J_3	343	85	85	27	85	135	Toppling	0.40	1.00	-25	0	75	II
J_4	20	83	60	10	83	133	Toppling	0.70	1.00	-25	0	42	III
W_{12}	133	28	54	57	28	-22	Wedge	0.15	0.4	-60	0	50	III
W_{13}	255	23	54	65	23	-27	Wedge	0.15	0.4	-60	0	50	III
W_{14}	109	9	54	81	9	-41	Wedge	0.15	0.15	-60	0	52	III

5. Discussion

The SMR geomechanical classification has been applied to three case studies, using the information derived from 3DPC and compared with the fieldwork data when available. This work focuses on how the SMR adjustment factors change, depending on the source of information and method used, and in the analysis of the main practical issues on the exploitation of 3DPC for calculating the SMR index, through three different case studies. For the first case study, the different discontinuity sets were extracted using different approaches. For case studies II and III, this information were complemented with the qualitative and quantitative information of the rock mass involved in the determination of the basic RMR. Finally, the SMR index was calculated through the geometric interpretation of the different failure mechanisms, including planar, wedge or toppling potential failures. The straightforward calculation of the auxiliary angles and the SMR geometric parameters were automatically performed using the SMRTool software.

In the first case study, it was discovered that, considering RMR_b as an independent variable, the use of 3D laser scanner data combined with DSE software can cause a variation in the SMR index. The comparison of the obtained results using DSE LiDAR with manual compass datasets, showed a variation of 31 units in slope 1 combined with W_{12}. This shows a difference in the slope stability depending on the approach used. More significant variations were found in J_3 combined with the three slopes (see Table 3).

The SMR index variations can be illustrated by analysing the discontinuity set J_3 and the slope 1, and are detailed in Table 3. . The highest difference is found

between the manual geological compass source data and the 3D laser scanner analysed, using DSE software. The obtained planes are (205/30) and (187/33) respectively, and the angle between their normal vectors is 9.8°. Despite this, the angle difference is acceptable for a mean plane, and its combination with slope 1 causes the A auxiliary angle to vary from 17° to 1° and therefore F_1 increases from 0.7 to 1. Moreover, dip values play a key role in this case. C auxiliary angle is equal to 118° in the first case, but it varies till 121° (only 3°) and thus, F_3 dwindle from -6 to -25. As a result, the product $F_1xF_2xF_3$ varies from -4.2 to -25, varying by one SMR class. Slightly better results will be obtained if the adjustment factors are calculated through the continuous functions [36], as this value varies from -2.5 to -19.2. Since the 3DPC from this case study is available in a public repository [31] the results of our research can be verified by other colleagues in order to validate our analysis and conclusions.

The second case study utilizes information derived from digital photogrammetry, 3D laser scanner and traditional methods. The result of this study shown in Table 4 indicates that, there is a good correlation between the SMR index calculated through fieldwork and 3D laser scanner data, and a discrepancy with those calculated through SfM data. Nevertheless, these results must be interpreted with caution, as the point cloud's quality acquired through SfM significantly depends on the camera used, the number and quality of the pictures, the acquisition strategy, the ground control points used, and the vertical and horizontal alignment of the raw 3DPC. The results compared to the different discontinuity sets, can be summarized as follows:

The first analysed DS (J_1) showed that, when using 3D laser scanning dataset, the SMR value is equal to 22, but when using the SfM of fieldwork collected data, the SMR value is equal to 26. A possible explanation for this fact might be that, though it is reasonable for normal vectors to be almost parallel , the slope's plane accounts for small variations in the orientation of the DS. This implies that SMR value variations can even change its geo-mechanical class.

The second DS (J_2) analysis, showed a significant variation in the SMR value. The SfM analysis shows an SMR value of 21, while laser scanning and fieldwork, show SMR values of 38. The most likely cause of the observed difference is that when using the SfM data, the A angle (see Table 2) is equal to 2° and thus $F_1 = 1$, but when using fieldwork and laser scanning dataset, this angle is higher than 10° so F_1 is 30% minority (see Table 4). In this case, the dip angle of J_2 is small, so its dip direction would vary easily, if the source data are inaccurate. This is the case of the sub-horizontal planes, where SfM was inaccurate because the digital pictures were taken with bias (horizontal line of sight and sub-horizontal DS). Moreover, these DS sub-horizontal orientation favour the accumulation of debris (some of them are partially or even completely covered) due to the progressive degradation of the material located at the upper part of the slope. Consequently, the 3D model does not modelize this flat surface correctly.

The third DS (J_3) analysis showed that the results of this calculation did not show any deviation.

The fourth DS (J_4) analysis evidenced a significant SMR value variation. A difference of 5 SMR units, was found, between fieldwork and 3D data, which was

caused by an angular difference of up to 20° between their dip direction. This deviation may be explained by the insufficient number of orientation measurements, which is due to the following reasons; On one hand, fieldwork campaign conditions are an important factor of this deviation because J_4 orientations were difficult to measure. On the other hand, the surface of exposed planes was small. These factors explain the fact that this DS had insufficient measurements to calculate the mean orientation with accuracy. Nevertheless, the use of 3DPC datasets, have increased the number of point measurements.

The analysis of all wedges (W_{ij}) also show differences, as they are defined by the intersection of previous pair of planes and then, are affected by the same sources of error.

The third case study applies the methodology in a singular rocky slope: a circular roundabout excavation in which the slope direction varies at different sectors of the slope. First of all, the discontinuity sets are extracted from a 3D laser scanning dataset using the DSE software, and the slope is modelled by means of a synthetic 3D point cloud. After this, the SMR index is computed for the different recognized DS, and the wedges derived from their combination (Table 5) and, then, the minimum SMR index envelope, is selected as a representative of the different orientations of the roundabout. The minimum computed SMR values, in which a high probability of failure exists, show a precise spatial coincidence with an existing planar rock slide (see Figures 3 e and f and 8f), which allows to validate the proposed approach, also demonstrating the reliability of SMR.

6. Conclusions

In recent times, the scientific community is showing an increasingly greater interest in the use of 3DPC for estimating mean plane orientations. The most significant findings that emerged from this study are:

Different methods of extracting DS, and different sources of information, can lead to different values of mean plane orientations, as was shown in case study I. Interestingly, these variations lead to higher or lower SMR values than those computed using conventional field methods. It was also shown that, the results strongly depend on the surface of information when the quantity of measurements is not enough (for example, when rock slopes are inaccessible because, fieldwork is risky) as was shown in case study II. Additionally, in accordance with case study I, it has been shown that in some cases, when orientations are affected by small variations, the SMR results can vary significantly and thus, the class can change. This fact points out the importance of a solid background in rock mechanics. Finally, this study has shown the reliability of SMR in predicting possible occurrence of failures, as it was shown in case study III.

In summary, the main advantages of the SMR index calculation (that is, the extraction of orientations on inaccessible or risky areas, quick calculation of the SMR adjustment factors, objectivity and reproducibility of the calculations, as well as reliability of this rock mass classification) in using a remote acquisition technique, leads us to think that this approach will be widely used in the forthcoming years.

7. Acknowledgements

This work was partially funded by the University of Alicante (vigrob-157 Project and GRE1404 Project), the Generalitat Valenciana (Projects GV/2011/044 and ACOMP/2014/136), the Spanish Ministry of Economy and Competitiveness (MINECO) and EU FEDER under Project TEC2011-28201-C02-02 and TIN2014-55413-C2-2-P. The 3D laser scanner used in this work for the 3D point cloud acquisition was acquired under the framework of the Programa Objetivo FEDER 2007-2013 Generalitat Valenciana - Unin Europea - Universidad de Alicante. Mr Javier Soler provided the pictures from the San Blas rock slope and the computer processing facilities. Finally, the authors would like to acknowledge Mr. Christopher Ward for the English language revision and correction of this manuscript.

8. References

[1] J. A. Hudson, J. P. Harrison, Engineering rock mechanics part 2: illustrative worked expamples: illustrative worked examples, Elsevier, 2001.

[2] Z. Bieniawski, Engineering classification of jointed rock masses, CIVIL ENGINEER IN SOUTH AFRICA 15 (12) (1973) 335–344.

[3] Z. T. Bieniawski, Engineering rock mass classifications: a complete manual for engineers and geologists in mining, civil, and petroleum engineering, John Wiley & Sons, 1989.

[4] N. Barton, R. Lien, J. Lunde, Engineering classification of rock masses for the design of tunnel support, Rock mechanics 6 (4) (1974) 189–236.

[5] L. I. G. de Vallejo, M. Ferrer, Geological engineering, CRC Press, 2011. URL https://www.crcpress.com/Geological-Engineering/Vallejo-Ferrer/9780415413527

[6] C. Irigaray, T. Fernández, J. Chacón, Preliminary rock-slope-susceptibility assessment using gis and the smr classification, Natural Hazards 30 (3) (2003) 309–324.

[7] M. Romana, New adjustment ratings for application of bieniawski classification to slopes, in: International symposium on the role of rock mechanics, Zacatecas, 1985, pp. 49–53.

[8] M. Romana, A geomechanical classification for slopes: slope mass rating, Comprehensive rock engineering 3 (1993) 575–599.

[9] F. Andrea, G. Andrea, M. Giuseppe, Rock slopes failure susceptibility analysis: from remote sensing measurements to geographic information system raster modules, American Journal of Environmental Sciences 6 (6) (2010) 489.

[10] A. Filipello, G. Mandrone, L. Bornaz, Structural data treatment to define rockfall susceptibility using long range laser scanner, in: G. Lollino, D. Giordan, K. Thuro, C. Carranza-Torres, F. Wu, P. Marinos, C. Delgado (Eds.), Engineering Geology for Society and Territory - Volume 6, Springer International Publishing, 2015, pp. 721–724. doi:10.1007/

978-3-319-09060-3_129.
URL http://dx.doi.org/10.1007/978-3-319-09060-3_129

[11] P. Alameda, Aplicación de nuevas metodologías de adquisición de datos para el análisis de estabilidad de taludes: casos de estudio en materiales foliados de la cordillera bética, Ph.D. thesis, University of Granada, Spain (2014).

[12] M. Jaboyedoff, T. Oppikofer, A. Abellán, M.-H. Derron, A. Loye, R. Metzger, A. Pedrazzini, Use of lidar in landslide investigations: a review, Natural hazards 61 (1) (2012) 5–28.

[13] A. Abellán, T. Oppikofer, M. Jaboyedoff, N. J. Rosser, M. Lim, M. J. Lato, Terrestrial laser scanning of rock slope instabilities, Earth Surface Processes and Landforms 39 (1) (2014) 80–97.

[14] S. Slob, B. van Knapen, R. Hack, K. Turner, J. Kemeny, Method for automated discontinuity analysis of rock slopes with three-dimensional laser scanning, Transportation Research Record: Journal of the Transportation Research Board 1913 (1) (2005) 187–194.

[15] M. I. Olariu, J. F. Ferguson, C. L. Aiken, X. Xu, Outcrop fracture characterization using terrestrial laser scanners: Deep-water jackfork sandstone at big rock quarry, arkansas, Geosphere 4 (1) (2008) 247–259.

[16] M. Sturzenegger, D. Stead, Quantifying discontinuity orientation and persistence on high mountain rock slopes and large landslides using terrestrial

remote sensing techniques, Natural Hazards and Earth System Science 9 (2) (2009) 267–287.

[17] A. Ferrero, G. Forlani, R. Roncella, H. Voyat, Advanced geostructural survey methods applied to rock mass characterization, Rock Mechanics and Rock Engineering 42 (4) (2009) 631–665. doi:10.1007/s00603-008-0010-4. URL http://dx.doi.org/10.1007/s00603-008-0010-4

[18] M. Sturzenegger, D. Stead, D. Elmo, Terrestrial remote sensing-based estimation of mean trace length, trace intensity and block size/shape, Engineering Geology 119 (3) (2011) 96–111.

[19] M. Jaboyedoff, R. Metzger, T. Oppikofer, R. Couture, M.-H. Derron, J. Locat, D. Turmel, New insight techniques to analyze rock-slope relief using dem and 3d-imaging cloud points: Coltop-3d software, in: T. . Francis (Ed.), Rock mechanics: Meeting Society's challenges and demands. Proceedings of the 1st Canada - U.S. Rock Mechanics Symposium, Vancouver, Canada, May 27-31, 2007, Vol. 1, 2007, pp. 61–68.

[20] K. Khoshelham, D. Altundag, D. Ngan-Tillard, M. Menenti, Influence of range measurement noise on roughness characterization of rock surfaces using terrestrial laser scanning, International Journal of Rock Mechanics and Mining Sciences 48 (8) (2011) 1215–1223.
URL http://www.sciencedirect.com/science/article/pii/S1365160911001456

[21] G. Gigli, N. Casagli, Semi-automatic extraction of rock mass structural data from high resolution lidar point clouds, International Journal of Rock Mechanics and Mining Sciences 48 (2) (2011) 187–198.

[22] M. J. Lato, M. Vöge, Automated mapping of rock discontinuities in 3d lidar and photogrammetry models, International Journal of Rock Mechanics and Mining Sciences 54 (2012) 150–158.

[23] A. J. Riquelme, A. Abellán, R. Tomás, M. Jaboyedoff, A new approach for semi-automatic rock mass joints recognition from 3d point clouds, Computers & Geosciences 68 (0) (2014) 38 – 52. doi:http://dx.doi.org/10.1016/j.cageo.2014.03.014.
URL http://www.sciencedirect.com/science/article/pii/S0098300414000740

[24] T. Oppikofer, M. Jaboyedoff, L. Blikra, M.-H. Derron, R. Metzger, Characterization and monitoring of the åknes rockslide using terrestrial laser scanning, Natural Hazards and Earth System Science 9 (3) (2009) 1003–1019.

[25] A. J. Riquelme, A. Abellán, R. Tomás, Discontinuity spacing analysis in rock masses using 3d point clouds, Engineering Geology 195 (2015) 185 – 195. doi:http://dx.doi.org/10.1016/j.enggeo.2015.06.009.
URL http://www.sciencedirect.com/science/article/pii/S0013795215002045

[26] M. Sturzenegger, D. Stead, Close-range terrestrial digital photogram-

metry and terrestrial laser scanning for discontinuity characterization on rock cuts, Engineering Geology 106 (34) (2009) 163 – 182. doi:http://dx.doi.org/10.1016/j.enggeo.2009.03.004.
URL http://www.sciencedirect.com/science/article/pii/S0013795209000556

[27] G. Umili, A. Ferrero, H. Einstein, A new method for automatic discontinuity traces sampling on rock mass 3d model, Computers & Geosciences 51 (0) (2013) 182 – 192. doi:http://dx.doi.org/10.1016/j.cageo.2012.07.026.
URL http://www.sciencedirect.com/science/article/pii/S0098300412002695

[28] W. C. Haneberg, et al., Directional roughness profiles from three-dimensional photogrammetric or laser scanner point clouds, in: E. Eberhardt, D. Stead, &T. Morrison (eds.), Rock Mechanics: Meeting Society's Challenges and Demands, 2007, pp. 101–106.
URL http://www.haneberg.com/downloadables/roughness_preprint.pdf

[29] T. Oppikofer, M. Jaboyedoff, A. Pedrazzini, M.-H. Derron, L. H. Blikra, Detailed dem analysis of a rockslide scar to characterize the basal sliding surface of active rockslides, Journal of Geophysical Research: Earth Surface 116 (F2) (2011) n/a–n/a. doi:10.1029/2010JF001807.
URL http://dx.doi.org/10.1029/2010JF001807

[30] M. J. Lato, G. Bevan, M. Fergusson, Gigapixel imaging and photogrammetry: Development of a new long range remote imaging technique, Remote Sensing 4 (10) (2012) 3006–3021.

[31] M. Lato, J. Kemeny, R. Harrap, G. Bevan, Rock bench: Establishing a common repository and standards for assessing rock-mass characteristics using lidar and photogrammetry, Computers & Geosciences 50 (0) (2013) 106 – 114, benchmark problems, datasets and methodologies for the computational geosciences. doi:http://dx.doi.org/10.1016/j.cageo.2012.06.014.
URL http://www.sciencedirect.com/science/article/pii/S0098300412002099

[32] A. Riquelme, A. Abellán, R. Tomás, SMRTool beta. A calculator for determining Slope Mass rating (SMR)., Online (June 2014).
URL http://personal.ua.es/en/ariquelme/smrtool.html

[33] R. Anbalagan, Landslide hazard evaluation and zonation mapping in mountainous terrain, Engineering geology 32 (4) (1992) 269–277.

[34] M. Romana, El papel de las clasificaciones geomecánicas en el estudio de la estabilidad de taludes, in: Actas del IV Simposio Nacional sobre taludes y laderas inestables, Vol. 3, 1997, pp. 955–1011.

[35] G. Leret Verdú, A. Lendínez González, I. Colondrón Gómez, M. del Olmo W., Magna 50 (2 serie) - Mapa Geològico de España a escala

1:50.000, hoja 871, Elda., online (1978).
URL http://www.igme.es/internet/cartografia/cartografia/magna50.asp?hoja=871&bis=

[36] R. Tomás, J. Delgado, J. Serón, Modification of slope mass rating (smr) by continuous functions, International Journal of Rock Mechanics and Mining Sciences 44 (7) (2007) 1062–1069.